SCIENTIFIC REPORTS

OPEN

Thermal efficiency of a thermocell made of Prussian blue analogues

Takayuki Shibata[1], Yuya Fukuzumi[2] & Yutaka Moritomo[2,3,4]

Received: 8 May 2018
Accepted: 21 September 2018
Published online: 03 October 2018

Recently, it was reported that a thermocell can convert temperature into electric energy by using the difference in the thermal coefficient ($\alpha = dV/dT$) of the redox potential (V) between the cathode and anode materials. Among battery materials, Prussian blue analogues (PBAs) are promising materials for thermocell, because α changes from approximately -0.3 mV/K in $Na_xMn[Fe(CN)_6]_{0.83}$ 3.5 H_2O (NMF83) to approximately 1.3 mV/K in $Na_xCo[Fe(CN)_6]_{0.9}2,9H_2O$ (NCF90). In this work, we systematically investigated the thermal efficiency (η) of the NMF83/NCF90 thermocell relative to the difference (ΔT) between low ($T_L = 282$ K) and high ($T_H = 292$–338 K) temperatures. We found that the thermal efficiency (η) increased proportionally with ΔT. The linear increase in η is ascribed to the linear increase in the cell voltage (V_{cell}) and the charge (Q_{NCF90}) extracted from NCF90. Moreover, η reached 3.19% at $\Delta T = 56$ K, which corresponds to 19% of the Carnot efficiency ($\eta_{carnot} = 17.0\%$). We further confirmed that the magnitude of Q_{NCF90} is quantitatively reproduced by the slopes of the discharge curves of NMF83 and NCF90.

A new thermoelectric technology, that converts waste heat near room temperature and/or human body heat to electric energy at low cost and high efficiency, is required for a "smart" society. A semiconductor-based thermoelectric device, that uses the so-called Seebeck effect, is a promising technology and is.applied for practical use in Peltier cooling and thermal power generation in space vehicles[1]. However, the current devices must be bulky and heavy to convert the temperature difference between the electrodes into a sufficient voltage, which is an inevitable disadvantage of the device.

Recently, several researchers[2–5] reported that a thermocell that uses the difference in the thermal coefficient ($\alpha = dV/dT$) of the redox potential (V) between the anode (α_{anode}) and cathode ($\alpha_{cathode}$) materials can convert the cell temperature (T_{cell}) into the electric energy. The thermocell can produce electric energy in the thermal cycle between low (T_L) and high (T_H) temperatures, making in share contract with the semiconductor-based thermoelectric device. Figure 1 shows a schematic of stages of the thermocell thermal cycle: (a) warming from T_L to T_H, (b) discharge at T_H, (c) cooling from T_H to T_L, and (d) discharge at T_L. In the (a) warming process, the redox potentials of the anode and cathode change by α_{anode} and α_{athode}, respectively. We expect a thermally induced change in V_{cell} as large as $\Delta T(\alpha_{cathode} - \alpha_{anode})$. In other words, electric energy is thermally stored in the thermocell. Some amount of the stored electric energy can be extracted by the (b) discharge process at T_H. During the (b) cooling process, the redox potentials of the anode and cathode change by $-\alpha_{anode}\,\Delta T$ and $-\alpha_{cathode}\,\Delta T$, respectively. The stored electric energy can be extracted by the (d) discharge process at T_L. Lee *et al.*[2] fabricated a thermocell with an anode and cathode made of $[Fe(CN)_6]^{3+}/[Fe(CN)_6]^{4+}$ [6] and a Prussian blue analogue (PBA) solid and succeeded in extracting electric energy. Yang *et al.*[3]. fabricated a thermocell with an anode and cathode made of Cu^{+}/Cu^{2+} [6] and a PBA solid and succeeded in extracting electric energy. Shibata *et al.*[5] fabricated a thermocell, consisting of two types of PBA solids with different α values. The thermocell produces electric energy with high thermal efficiency ($\eta = 1\%$) between T_H (=295 K) and T_H (=323 K). This type of thermocell extends the application range of the battery materials from energy storage to energy conversion.

PBAs with chemical formulae are of $Li_xM[Fe(CN)_6]_y$ and $Na_xM[Fe(CN)_6]_y$ (M = transition metal) are promising candidates for cathode materials in lithium-ion and sodium-ion secondary batteries[7–16]. Most of the PBA materials have face-centrered cubic (fcc) ($Fm\bar{3}m$; $Z = 4$) or trigonal ($R\bar{3}m$; $Z = 3$) structures[17], consisting of a three-dimensional (3D) jungle-gym-type host framework with guest Li^{+}/Na^{+} ions and H_2O molecules, which are accommodated in the nanopores of the framework. The framework contains considerable $[Fe(CN)_6]$ vacancies

[1]National Institute of Technology, Gunma College, Maebashi, Gunma, 371–8530, Japan. [2]Graduate School of Pure and Applied Sciences, University of Tsukuba, Tsukuba, 305–8571, Japan. [3]Faculty of Pure and Applied Sciences, University of Tsukuba, Tsukuba, 305–8571, Japan. [4]Tsukuba Research Center for Energy Materials Science (TREMS), University of Tsukuba, Tsukuba, 305–8571, Japan. Correspondence and requests for materials should be addressed to Y.M. (email: moritomo.yutaka.gf@u.tsukuba.ac.jp)

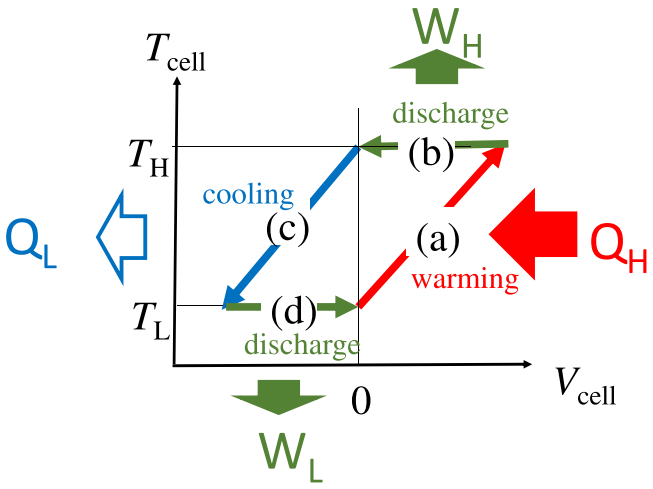

Figure 1. Schematic illustration of thermal cycle vs. voltage (V_{cell}) and temperature (T_{cell}) of the thermocell. The cycle consists of four processes. (**a**) Heating from T_L to T_H, (**b**) discharge at T_H, (**c**) cooling from T_H to T_L, and (**d**) discharge at T_L. Processes (**a**) and (**c**) are performed in the open circuit condition. Q_H and Q_L are the inflow and outflow of heat, respectively, and W_H and W_L are the electric works at T_H and T_L, respectively.

(10–30%). The discharge curves of Co- and Mn-PBAs show characteristic plateaus, the redox reaction of which are well assigned using X-ray absorption spectroscopy[18,19]. PBAs are also promising materials for thermocells because the magnitude and sign of α can be controlled by the chemical composition[20]. The α values of $Na_xCo[Fe(CN)_6]_{0.9}2{,}9H_2O$ (NCF90) in the lower-lying plateau and the value of $Na_xCo[Fe(CN)_6]_{0.71}3.6H_2O$ (NCF71) are ~1.3 and ~0.7 mV/K, respectively. Interestingly, the α of $Na_xMn[Fe(CN)_6]_{0.83}$ $3.5H_2O$ (NMF83) in the lower-lying plateau is negative (approximately − 0.3 mV/K).

In our previous work[5], we demonstrated that the NCF71/NCF90 thermocell can convert temperature into electric energy with 1% thermal efficiency between $T_L = 295$ K and $T_H = 323$ K. In this work, we systematically investigated the thermal efficiency (η) of the NMF83/NCF90 thermocell against the temperature difference (ΔT) between T_L and T_H. The η of the NMF83/NCF90 thermocell is expected to be higher than that of the NCF71/NCF90 thermocell because $\Delta\alpha$ ($=\alpha_{cathode} - \alpha_{anode} \sim 1.7$ mV/K) is much larger in the former cell. We found that η increases in proportion to ΔT and reaches 3.19% at $\Delta T = 56$ K. The linear increase in η is ascribed to the linear increase in the cell voltage (V_{cell}) and charge (Q_{NCF90}) extracted from NCF90. We further confirmed that the magnitude of Q_{NCF90} is quantitatively reproduced by the slopes of the discharge curves in NMF83 and NCF90.

Discharge curve of a half–cell

Figure 2 shows the discharge curves of the (a) NMF83 and (b) NCF90 films. The curve of NMF83 [(a)] shows two plateaus (plateaus I and II) near 1.1 and 0.6 V vs. Ag/AgCl. Plateau I (<20 mAh/g) near 1.1 V is ascribed to the reaction[19]: $Mn^{3+}{}_{0.49}Mn^{2+}{}_{0.51}[Fe^{3+}(CN)_6]_{0.83} + 0.49Na^+ + 0.49\,e^- \rightarrow Na_{0.49}Mn^{2+}[Fe^{3+}(CN)_6]_{0.83}$. Plateau II (>20 mAh/g) near 0.6 V is ascribed to the reaction: $Na_{0.49}Mn^{2+}[Fe^{3+}(CN)_6]_{0.83} + 0.83Na^+ + 0.83\,e^- \rightarrow Na_{1.32}Mn^{2+}[Fe^{2+}(CN)_6]_{0.83}$. In the discharge process, Na^+ ions are inserted into the framework, which causes reduction of Mn^{3+}/Fe^{3+} to maintain the charge neutrality. The curve of NCF90 [(b)] shows two plateaus (plateaus III and VI) near 1.0 and 0.5 V vs. Ag/AgCl. Plateau III (<50 mAh/g) near 1.0 V is ascribed to the reaction:[18] $Co^{3+}[Fe^{3+}(CN)_6]_{0.6}[Fe^{2+}(CN)_6]_{0.3} + 0.6Na^+ + 0.6\,e^- \rightarrow Na_{0.6}Co^{3+}[Fe^{2+}(CN)_6]_{0.9}$. Plateau VI (>50 mAh/g) near 0.5 V is ascribed to the reaction: $Na_{0.6}Co^{3+}[Fe^{2+}(CN)_6]_{0.9} + Na^+ + e^- \rightarrow Na_{1.6}Co^{2+}[Fe^{2+}(CN)_6]_{0.9}$.

The difference ($\Delta\alpha = \alpha_{cathode} - \alpha_{anode}$) in α is a crucial parameter for a thermocell, because V_{cell} increases in proportion to $\Delta\alpha$. Fukuzumi *et al.*[20] systematically investigated the α values of prototypical PBAs against the Na concentration (x). In NMF83, α gradually decreases from 1.4 to − 0.4 mV/K with increasing in x. At plateau II, α becomes negative (approxmately −0.3 mV/K). In NCF90, α is ~0.4 mV/K and ~1.3 mV/K in plateau III and IV, respectively. Therefore, we can maximize $\Delta\alpha$ if we chose NMF83 (plateau IV) and NCF90 (plateau II) as the anode and cathode, respectively. As discussed later, the slope of the plateau is another crucial parameter. In this work, we define the discharge curves of NMF83 [Fig. 1(a)] and NCF90 [Fig. 1(b)] as $V_{NMF83}(Q)$ and $V_{NCF90}(Q)$, respectively. The slopes, *i.e.*, dV_{NMF83}/dQ and dV_{NCF90}/dQ, are roughly evaluated as −3.5 and −0.5 mV/(mAh/g) at plateaus II and IV, respectively.

Thermal Cycle Measurement of Thermocell

We fabricated a two-pole beaker-type thermocell; for this thermocell, the anode, cathode and electrolyte are an as-grown NMF83 film, pre-oxidized NCF90 film, and an aqueous solutions containing 17 mol/kg $NaClO_4$, respectively. The as-prepared thermocell was slowly cooled down to T_L (=282 K). At T_L, the thermocell shows a finite V_{cell} (~0.1 V), which was discharged to 0 V under the constant current condition. If T_{cell} is slowly increased by $\Delta T (= T_H - T_L)$ in the open circuit condition, the redox potentials of the anode and cathode change by $\alpha_{anode}\Delta T$ and $\alpha_{cathode}\Delta T$, respectively, in the warming process. We expect a thermally induced change in V_{cell} as larger as $\Delta T(\alpha_{cathode} - \alpha_{anode})$. In other words, the electric energy is thermally stored in the thermocell. The amount of stored electric energy can be evaluated by the discharge process to 0 V under a constant current condition. The

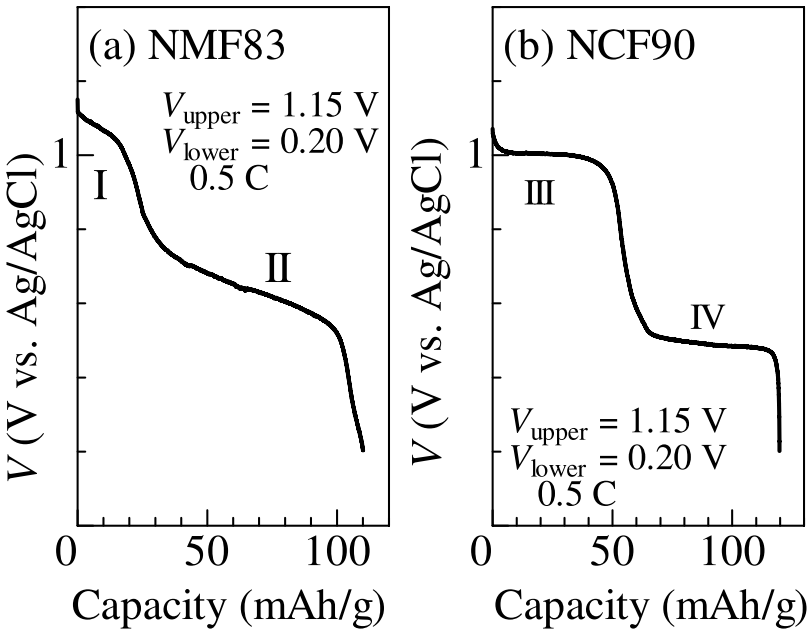

Figure 2. Discharge curves of (**a**) $Na_xMn[Fe(CN)_6]_{0.83}$ $3.5H_2O$ (NMF83) and (**b**) $Na_xCo[Fe(CN)_6]_{0.9}2.9H_2O$ (NCF90) films measured at 0.5 C. For convenience of explanation, we defined plateaus I, II, III, and IV.

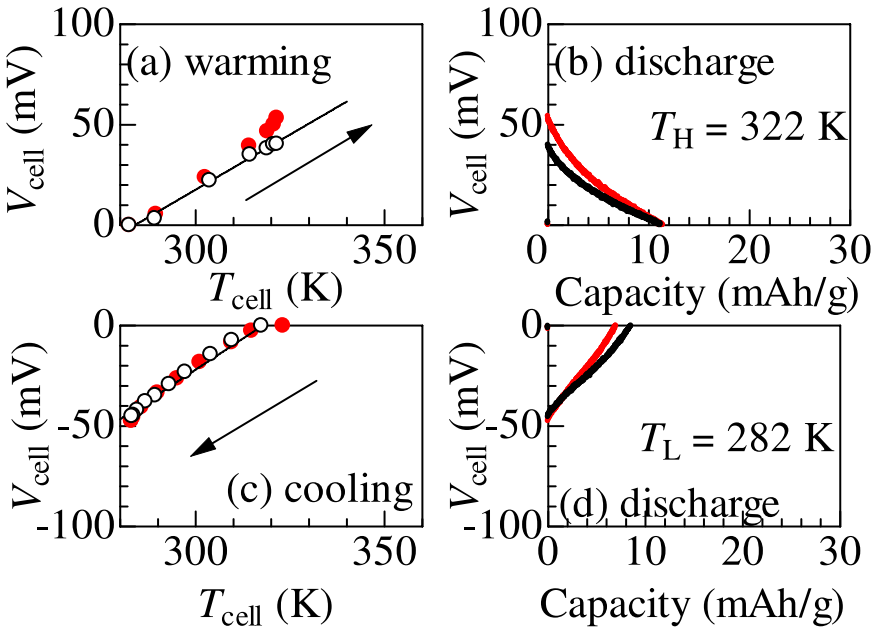

Figure 3. Temperature (T_{cell}) and voltage (V_{cell}) of the NCF83/NCF90 thermocell in the respective processes of the thermal cycle at $\Delta T = 40$ K. (**a**) Warming process from T_L (=282 K) to T_H (=322 K) in the open circuit condition, (**b**) discharge process at T_H at constant current ($I = 1.1\,\mu A$), (**c**) cooling process from T_H to T_L in the open circuit condition, and (**d**) discharge process at T_L at constant current ($I = -1.1\,\mu A$). Black and red colours represent the data obtained in the first and second cycles, respectively.

sweep area on the voltage-charge diagram corresponds to the stored electric energy. The behaviour of V_{cell} in the cooling process is opposite to that in the warming process. In this cooling process, the redox potentials of the anode and cathode change by $-\alpha_{anode}\Delta T$ and $-\alpha_{cathode}\Delta T$, respectively. We expect a thermally induced change in V_{cell} as larger as $-\Delta T(\alpha_{cathode} - \alpha_{anode})$. The stored electric energy can be extracted by the discharge process to 0 V under constant current condition. Therefore, our thermocell can convert temperature to electric energy in the thermal cycle between T_L and T_H.

Figure 3 shows a prototypical example of the thermal cycle of the NMF83/NCF90 thermocell at $\Delta T = 40$ K. Black and red colours represent the data obtained in the first and second cycles, respectively. In the (a) warming

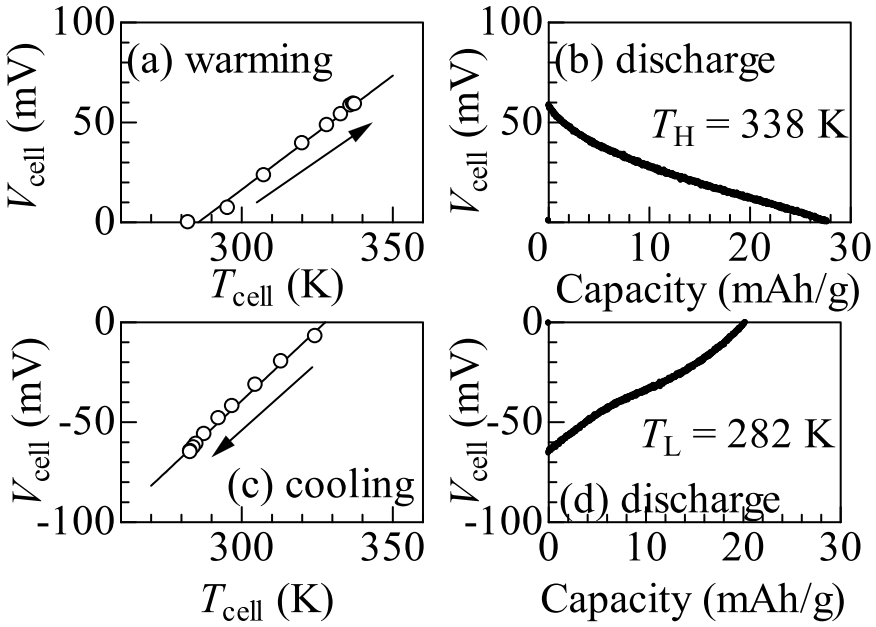

Figure 4. Thermal cycle ($\Delta T = 56$ K) of the NCF83/NCF90 thermocell: (**a**) Warming process from T_L (=282 K) to T_H (=338 K) in the open circuit condition, (**b**) discharge process at T_H at constant current ($I = 0.6\,\mu$A), (**c**) cooling process from T_H to T_L in the open circuit condition, and (**d**) discharge process at T_L at constant current ($I = -0.6\,\mu$A).

process, V_{cell} linearly increases with the increase in T_{cell} at a rate of 1.2 mV/K. The rate is comparable to $\Delta\alpha$ (~1.6 mV/K). At T_H, the cell shows a finite voltage ($V_{cell} = 40$ mV), i.e., the cell is thermally-charged. In the (b) discharge process at T_H, V_{cell} linearly decreases with the extracted charge. The final extracted charge (Q_{NCF90}) from NCF90 is11.3 mAh/g, which is 10.8% of the discharge curve of NCF90 [Fig., 1(b)]. The electric work ($W_H = 3.29$ meV/NCF90) at T_H is roughly evaluated by $qV_{cell}/2$, where q is the final extracted charge per NCF90. In the (c) cooling process, V_{cell} linearly decreases with the decrease in T_{cell} at a rate of 1.3 mV/K. At T_L, the cell shows a finite voltage ($V_{cell} = -44$ mV). In the (d) discharge process, Q_{NCF90} was 8.4 mAh/g. The electric work (W_L) at T_L is 2.82 meV/NCF90. The data in the second cycle are highly similar to those in the first cycle.

Figure 4 shows another example of the thermal cycle at $\Delta T = 56$ K. In the (a) warming process, V_{cell} linearly increases with the increase in T_{cell} at a rate of 1.1 mV/K. At T_H (=338 K), the cell shows a finite voltage ($V_{cell} = 60$ mV). In the (b) discharge process at T_H, V_{cell} linearly decreases with the extracted charge, where Q_{NCF90} is 28.0 mAh/g, which is 26.7% of the discharge curve of NCF90 [Fig. 1(b)], and W_H is 12.80 meV/NCF90. In the (c) cooling process, V_{cell} linearly decreases with the decrease in T_{cell} at a rate of 1.2 mV/K. At T_L (=282 K), the cell shows a finite voltage ($V_{cell} = -65$ mV). In the (d) discharge process, Q_{NCF90} is 20.0 mAh/g and W_L is 9.70 meV/NCF90. Figure S1 shows the discharge curves at T_H and T_L against ΔT.

Thermal Efficiency Against ΔT

The thermal efficiency (η) is defined by $W_H + W_L/Q_H$, where Q_H is the inflow of heat. Table 1 shows W_H, W_L, Q_H, and η against ΔT. Furthermore, W_H (W_L) was roughly evaluated as $qV_{cell}/2$ at T_H (T_L), where q is the final extracted charge per NCF90 in the discharge process at T_H (T_L) and Q_H was evaluated as $(C_{anode} + C_{cathode})\Delta T$, where C_{anode} ($C_{cathode}$) is the heat capacity of anode (cathode) material. We neglected the heat capacity of the electrolyte because the amount of electrolyte is minimized in the current thermocell made of redox-capable solids. Using the specific heat (=4.16 meV/K per formula unit) of the ideal $Na_2Co[Fe(CN)_6]$ in the Dulong-Petit law, Q_H is expressed as $4.16(1 + n)\Delta T$ per NCF90, where n [$=n_{NMF83}/n_{NCF90}$. where n_{NMF83} (n_{NCF90}) is the number of the the NMF83 (NCF90) units] is the molar ratio. Additionally, W_H, W_L, Q_H, and η monotonously increases with ΔT, and η reaches 3.19% at $\Delta T = 56$ K, which corresponds to19% of the Carnot efficiency ($\eta_{carnot} = 17.0\%$).

Comparison with Previous Works

In Table 2, we compare the cell parameters and η in the current thermocell with those in previously reported thermocells. In the thermocells reported in ref.[2] and ref.[3], ehe electrolyte is different between the anode and cathode and is separated by a membrane. However, the thermocells made of two types of PBA solids (ref.[5] and this work) use the same electrolyte in the anode and cathode. As discussed in the following section, η increases linearly with ΔT. We should compare $\eta/\Delta T$, rather than η, among the thermocells, and the $\eta/\Delta T$ values of the thermocells made of PBA solids are comparable to those of the thermocells reported in ref.[2] and ref.[3].

In the thermocells made of PBA solids, $\eta/\Delta T$ (=0.07%/K) in the NMF83/NCF90 thermocell is much higher than that (=0.04%/K) in the NCF71/NCF90 thermocell. The enhancement of $\eta/\Delta T$ is ascribed to the larger $\Delta\alpha$ in the NMF83/NCF90 thermocell. Specifically, $\Delta\alpha$ is ~ 1.6 and 0.53 mV/K for the NMF83/NCF90 and NCF71/NCF90 thermocell, respectively.

Cycle	ΔT (K)	W_H(meV/NCF90)	W_L(meV/NCF90)	d_{NCF90} (mm)	d_{NMF83} (mm)	n	Q_H(meV/NCF90)	η (%)
First	10	0.20	0.12	0.80	0.86	1.19	91.1	0.35
First	20	0.50	0.67	0.80	0.86	1.19	182.2	0.64
First	30	1.45	1.37	0.76	0.75	1.09	260.8	1.08
Second	30	0.98	1.23				260.8	0.85
First	39	3.07	2.58	0.42	0.49	1.27	368.3	1.53
Second	39	4.03	2.16				368.3	1.65
First	51	7.09	4.42	0.71	0.80	1.25	477.4	2.41
First	56	12.80	9.90	0.40	0.74	2.05	710.5	3.19

Table 1. Parameters and performance of the NMF83/NCF90 thermocell. n [$=n_{NMF83}/n_{NCF90}$. where n_{NMF83} (n_{NCF90}) is the number of NCF83 (NCF90) units] is the molar ratio. d_{NCF90} (d_{NCF90}) is the thickness of the NMF83 (NCF90) film, and W_H (W_L) and Q_H are the electric works at T_H (T_L) and the inflow of heat, respectively.

Anode	Cathode	α_{anode} (mV/K)	$\alpha_{cathode}$ (mV/K)	η (%)	ΔT (K)	$\eta/\Delta T$ (%)	Ref.
CuHCF	Cu/Cu^{2+}	−0.36	0.83	5.7	50	0.11	[2]
$Fe(CN)_6^{3-}/Fe(CN)_6^{4-}$	$KFe[Fe(CN)_6]$	−1.46	0.00	2.0	40	0.05	[3]
NCF71	NCF90	0.53	1.32	1.0	28	0.04	[5]
NMF83	NCF90	−0.3[20)]	1.3[20)]	3.2	56	0.07	This work

Table 2. Comparison of the parameters and thermal efficiency (η) of the thermocell. ΔT is the difference between T_H and T_L, and α_{anode} and $\alpha_{cathode}$ are the thermal coefficients of the redox potential of the anode and cathode, respectively.

Discussion

We turn the discussion to the ΔT dependence of V_{cell}, Q_{NCF90}, and η. Figure 5(a) shows the ΔT dependence of V_{cell}. The open and closed circles represent the data at T_H and T_L, respectively, and V_{cell} increases linearly with ΔT, as indicated by the solid line. The coefficient (=1.15 mV/K) is comparable to $\alpha_{NCF90} - \alpha_{NMF83}$ (~ 1.6 mV/K). Thus, we experimentally confirm the relationship of $V_{cell} = \Delta T(\alpha_{NCF90} - \alpha_{NMF83})$.

Figure 5(b) shows the ΔT dependence of Q_{NCF90}. The open and closed circles represent the data at T_H and T_L, respectively. We quantitatively evaluate Q_{NCF90} at T_H from the discharge curves, V_{NMF83}(Q) and V_{NMF83}(Q), of NMF83 and NCF90. By applying the Tayloer expansion, V_{cell} at T_H is expressed as $Q_{NCF90}dV_{NCF90}/dQ + (-Q_{NNF83}dV_{NMF83}/dQ)$, where Q_{NCF90} (Q_{NMF83}) is the final extracted charges from NCF90 (NMF83). The first and second terms are negative, because $dV_{NCF90}/dQ < 0$, $dV_{NMF83}/dQ < 0$, and $Q_{NMF83} < 0$. The charge neutrality between the anode and cathode imposes a constraint condition of $m_{NMF83}Q_{NMF83} = -m_{NCF90}Q_{NCF90}$, where m_{NMF83} (m_{NCF90}) is the mass of NMF83 (NCF90). We obtaine $Q_{NCF90} = -V_{cell}/(dV_{NCF90}/dQ + m^{-1}dV_{NMF83}/dQ)$, where $m = m_{NMF83}/m_{NCF90}$. We note that $m = n$ (M_{NMF83}/M_{NCF90}), where M_{NMF83} (=338.5) and M_{NCF90} (=324.0) are the molecular weights of NMF83 and NCF90, respectively, and dV_{NMF83}/dQ and dV_{NCF90}/dQ are roughly evaluated as −3.5 and −0.5 mV/(mAh/g). In Fig. 5(b), these calculated Q_{NCF90} values at T_H are plotted with crosses. The calculated Q_{NCF90} satisfactorily reproduces the experimentally-obtained Q_{NCF90}. We further confirmed the strong correlation between the calculated and experimentally-obtained Q_{NCF90} data at T_L (Fig. S2), thus, we demonstrating the empirical relationship of $Q_{NCF90} = -V_{cell}/(dV_{NCF90}/dQ + m^{-1}dV_{NMF83}/dQ)$. These arguments clearly indicate that the slope of the discharge curve is a determining parameter of Q_{NCF90}. In other words, the flatter the discharge curve becomes, the higher η becomes.

Figure 5(c) shows the ΔT dependence of η, where η linearly increase with ΔT, as indicated by the solid line., because V_{cell} [$=\Delta T(\alpha_{NCF90} - \alpha_{NMF83})$], Q_{NCF90} [$=-V_{cell}/(dV_{NCF90}/dQ + m^{-1}dV_{NMF83}/dQ)$] and Q_H increases in proportion to ΔT.

Summary

We systematically investigated V_{cell}, Q_{NCF90}, and η of the NMF83/NCF90 thermocell against ΔT. These three quantities increase linearly with ΔT, and η reaches 3.19% at $\Delta T = 56$ K, which corresponds to 19% of the Carnot efficiency ($\eta_{carnot} = 17.0\%$). We further confirmed that the magnitude of Q_{NCF90} is quantitatively reproduced by the slopes of the discharge curves of NMF83 and NCF90. These observations unambiguously illustrate us the strategy for enhancing η of the thermocell, that is, to explore and/or develop materials with a higher $|\alpha|$ and a flatter discharge curve.

Method

Fabrication and characterization of NMF83 and NCF90 films. Thin films of $Na_xMn[Fe(CN)_6]_{0.83}$ $3.5H_2O$ (NMF83) and $Na_xCo[Fe(CN)_6]_{0.9}2{,}9H_2O$ (NCF90) were synthesized by electrochemical deposition on an indium tin oxide (ITO) transparent electrode. Details of the synthesis conditions are described in literature[19,21]. The film area was 1.0 cm^2. The NMF83 film consists of crystalline particles of a few hundred nm and the colour is white. The NCF90 film also consists of crystalline particles of a few hundred nm and the colour is light green.

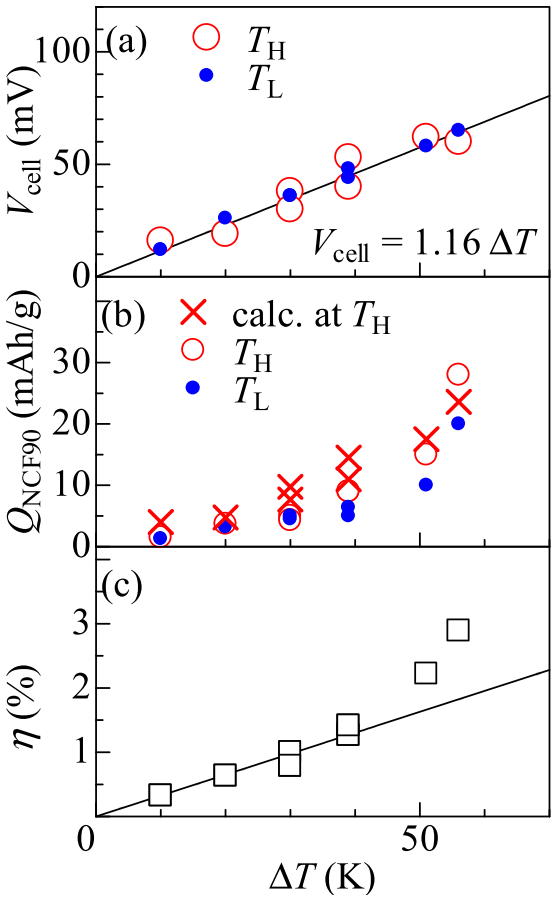

Figure 5. ΔT dependence of the (**a**) cell voltage (V_{cell}), (**b**) final extracted charge (Q_{NCF90}) from NCF90, and (**c**) thermal efficiency (η). The open and closed circles in (**a**) and (**b**) represent the data at T_H and T_L, respectively. The solid lines in (**a**) and (**c**) indicate the results of least-squares fitting. The crosses in (**b**) are values calculated from the discharge curves of NMF83 and NCF90.

The film thicknesses were determined by a profilometer (BRUKER Dektak3030). The chemical composition of the film was determined by the inductively coupled plasma (ICP) method and CHN organic elemental analysis.

The synchrotron radiation X-ray powder diffraction (XRD) measurements were performed at BL02B2 beamline[22] at the SPring-8. The films were removed from the ITO glass and were filled in 300 μm glass capillaries. The capillary was placed at the Debye Scherrer camera. The XRD patterns were monitored with a one-dimensional semiconductor detector (MYTHEN, Dectries Ltd.). The exposure time was 5 min. The wavelength of the X-rays (=0.69963 Å) was calibrated by the cell parameter of a standard CeO_2 powder. Figure S3 shows the magnified diffraction pattern of NMF83 and NCF90. All reflections in NMF83 are assigned to a face-centrered cubic (fcc) structure ($Fm\bar{3}m$; $Z = 4$), whereas those in NCF90 are assigned to a trigonal (hexagonal setting) structure ($R\bar{3}m$; $Z = 3$). The cell parameters were refined using the Rietan-PF program[23], and $a = 10.5210(2)$ Å in NMF83, $a_H = 7.4353(4)$ Å and $c_H = 17.4758(11)$ Å in NCF90.

The charge/discharge curves of the NMF83 and NCF90 films were measured with a potentiostat (HokutoDENKO HJ1001SD8) using a three-pole beaker-type cell. The working, referential, and counter electrodes were the PBA film, a standard Ag/AgCl electrode, and Pt, respectively. The electrolytes consisted of aqueous solutions containing 17 mol/kg $NaClO_4$. The charge/discharge rate was 0.5 C. The cut-off voltage was ranged from 0.20 to 1.15 V vs. Ag/AgCl. The mass of each film was evaluated using thickness, area, and density. We confirmed that the actual densities of the NMF83 and NCF90 films were 0.71 and 0.58 of the ideal density, respectively.

Thermal cycle measurement of thermocell. The thermocell is a two-pole beaker-type cell (Fig. S4). The anode, cathode and electrolyte are the as-grown NMF83 film, pre-oxidized NCF90 film, and aqueous solutions containing 17 mol/kg $NaClO_4$, respectively. Pre-oxidization of the NCF90 film was performed at $V_{upper} = 0.65$ V against Ag/AgCl in aqueous solutions containing 17 mol/kg $NaClO_4$. The as-prepared thermocell was slowly cooled to T_L (=282 K). At T_L, the thermocell show a finite V_{cell} (~0.1 V), which was discharged to 0 V under a constant current condition (0.1 C). The discharge rate was defined by the inverse of the charging time [hour] of the NCF90 film.

The thermal cycle measurement consists of four processes: (a) warming process from T_L to T_H, (b) discharge process at T_H, (c) cooling process from T_H to T_L, and (d) discharge process at T_L. In the (a) warming process, T_{cell}

was slowly increased from T_L to T_H in the open circuit condition, and T_{cell} was monitored by a platinum resistance thermometer in the electrolyte. At (b) T_H, the thermally-charged cell was discharged at 0.1 C. In the (c) cooling process, T_{cell} was slowly decreased from T_H to T_L in the open circuit condition. At (d) T_L, the thermally-charged cell was discharged at 0.1 C. T_L was fixed at 282 K and T_H was changed from 292 K to 338 K.

References

1. Goldsmid, H. J. *Introduction to Thermoelectricity*, Springer-Verlag, Berlin, 2010.
2. Lee, S. W. *et al*. An electrochemical system for efficiently harvesting low-grade heat energy. *Nat. Commun.* **5**, 3942 (2014).
3. Yang, Y. *et al*. Charging-free electrochemical system for harvesting low-grade thermal energy. *PNAS* **111**, 17011–17116 (2014).
4. Wang, J. *et al*. Thermal charging phenomenon in electrical double layer capacitors. *Nano Lett.* **15**, 5784–5790 (2015).
5. Shibata, T., Fukuzumi, Y., Kobayashi, W. & Moritomo, Y. Thermal power generation during heat cycle near room temperature. *Appl. Phys. Express* **11**, 017101 (2018).
6. Quickenden, T. I. & Mua, Y. The power conversion efficiencies of a thermogalvanic cell operated in three different orientations. *Electrochem. Soc.* **142**, 3652–3669 (1995).
7. Matsuda, T. & Moritomo, Y. Thin film electrode of Prussian blue analogue for Li-ion battery. *Appl. Phys. Express* **4**, 047101 (2011).
8. Moritomo, Y., Takachi, M., Kurihara, Y. & Matsuda, T. Thin film electrodes of Prussian blue analogues with rapid Li^+ intercalation. *Appl. Phys. Express* **5**, 041801 (2012).
9. Takachi, M., Matsuda, T. & Moritomo, Y. Structural, Electronic, and Electrochemical Properties of $Li_xCo[Fe(CN)_6]_{0.90}2.9H_2O$. *Jpn. J. Appl. Phys.* **52**, 044301 (2013).
10. Lu, Y., Wang, L., Cheng, J. & Goodenough, J. B. Prussian blue: a new framework of electrode materials for sodium batteries. *Chem. Commun.* **48**, 6544–6546 (2012).
11. Takachi, M., Matsuda, T. & Moritomo, Y. Cobalt hexacyanoferrate as cathode material for Na^+ secondary battery. *Appl. Phys. Express* **6**, 025802 (2013).
12. Yang, D. *et al*. Structure optimization of Prussian blue analogue cathode materials for advanced sodium ion batteries. *Chem. Commum.* **50**, 13377–13380 (2014).
13. Lee, H. W. *et al*. Manganese hexacyanomanganate open framework as a high-capacity positive electrode material for sodium-ion batteries. *Nat. Commun.* **5**, 5280 (2014).
14. Wang, L. *et al*. Rhombohedral Prussian white as cathode for rechargeable sodium-ion batteries. *J. Am. Chem. Soc* **137**, 2548–2554 (2015).
15. Yu, S. *et al*. A promising cathode material of sodium iron-nickel hexacyanoferrate for sodium ion batteries. *J. Power Sources* **275**, 45–49 (2015).
16. You, Y., Wu, X.-L., Yin, Y.-X. & Guo, Y.-G. High-quality Prussian blue crystals as superior cathode materials for room-temperature sodium-ion batteries. *Energy Environ. Sci.* **7**, 1643–1647 (2014).
17. Niwa, H., Kobayashi, W., Shibata, T., Nitani, H. & Moritomo, Y. *Invariant nature of substituted element in metal-hexacyanoferrate. Sci. Reps.* **7**, 13225 (2017).
18. Takachi, M., Matsuda, T. & Moritomo, Y. Redox reactions in Prussian blue analogue films with fast Na^+ intercalation. *Jpn. J. Appl. Phys.* **52**, 090202 (2013).
19. Matsuda, T., Takachi, M. & Moritomo, Y. A sodium manganese ferrocyanide thin film for Na-ion batteries. *Chem. Commun.* **49**, 2750–2752 (2013).
20. Fukuzumi, Y., Amaha, K., Niwa, H., Kobayashi, W. & Moritomo. Y. Prussian blue analogues as promising thermal power generation materials. *Energy Technol.* **6**, 1–7 (2018).
21. Igarashi, K., Nakada, F. & Moritomo, Y. Electronic structure of hole-doped Co-Fe cyanides: $Na_{1.60-\delta}Co[Fe(CN)_6]_{0.90}$ $2.9H_2O$ ($0.0 \leq \delta \leq 0.85$). *Phys. Rev. B* **78**, 235106 (2008).
22. Nishibori, E. *et al*. The large Debye-Scherrer camera installed at SPring-8 BL02B2 for charge density studies. *Nucl. Instrum. Methods Phys. Res.* **A467-468**, 1045–1048 (2001).
23. Izumi, F. & Momma, K. Three-dimensional visualization in powder diffraction. *J. Solid State Phenom.* **130**, 15–20 (2007).

Acknowledgements

This work was supported by JSPS KAKENHI (Grant Number JP17H0113) and the Japan Prize Foundation. The synchrotron radiation experiments were performed at BL02B2 of SPring-8 with the approval of the Japan Synchrotron Radiation Research Institute (JASRI) (Proposal No. 2017A1040 and 2017A1649). The elemental analyses were performed at the Chemical Analysis Division, Research Facility Center for Science and Engineering, University of Tsukuba.

Author Contributions

T.S. performed the electrochemical measurements and thermal cycle measurements. Y.F. fabricated and characterized the PBA films. Y.M planned the overall investigation and wrote the manuscript.

Additional Information

Supplementary information accompanies this paper at https://doi.org/10.1038/s41598-018-33091-w.

Competing Interests: The authors declare no competing interests.

Publisher's note: Springer Nature remains neutral with regard to jurisdictional claims in published maps and institutional affiliations.